



Numerical Analysis to Evaluate the Behavior of the Concrete-Filled Hollow Steel Tubular Columns

Yasser R. Tawfic ⁽¹⁾, Ahmad Saudi A. Sayed ⁽²⁾, L. M. Abdel-Hafez ⁽³⁾, Mohamed A. Eid ⁽⁴⁾

Civil Dept., Faculty of Eng., Minia University ⁽¹⁾

Higher Institute of Engineering and Technology, New Minia, Egypt ⁽²⁾

Minia University ⁽³⁾ Minia University ⁽⁴⁾

a.saudi@mhiet.edu.eg

Abstract

Concrete-filled hollow steel tubular (CFHST) columns have become appropriate solution for the construction of offshore platform supports, columns for large industrial workshops, as well as high rise buildings. In this research, a numerical study was conducted to investigate the optimal design of the CFHST columns. The numerical study comprises two phases: verification of experimental work using a nonlinear finite element software ANSYS 18.1 and a parametric study on the behavior of 33 full-scale CFHST columns. The cross-sectional shape, the depth to width (t_s/b_s) ratio, the slenderness ratio, and the distribution of the total steel area through the concrete core and the steel tube were the main variables. The reinforcement of the concrete core as well as the confinement of the external steel tube enhanced the ultimate loads, stiffness, and ductility of the CFHST columns. The Use of 4% internal longitudinal steel reinforcements for the CFHST columns results in up to 30 % increase for the values of the ultimate loads.

Keywords: Confinement, hollow steel tube, Cross-sectional shape, ductility

1. Introduction

The development of the construction and the spread of high buildings led to the use of composite reinforced concrete sections. Concrete-filled hollow steel tubular CFHST column is a structural component that combines a steel tube with a plain or reinforced concrete core to enhance the load bearing capability. The concrete-external steel tube interaction results in a cost-effective and highly efficient member among the wide range of structural elements in building and bridge construction [1–6]. Numerous benefits of CFHST columns include their high load-carrying capacity, high ductility, high energy absorption capacity, and quick construction. Considering different variables such as the length to diameter ratio, the cross-sectional shape, and the partial compression area, Yang and Han et al.

[7] examined the behavior of CFHST columns under partial compression. Twenty-six CFHST column specimens were tested as part of the investigation, and the behavior of each specimen was confirmed by establishing a finite element model using ABAQUS software. According to the study, partially compressed CFHST columns behave in a manner that is comparable to fully compressed CFHST columns.

The compressive behavior of circular CFHST sections with a separation gap between the concrete and the exterior steel tube was researched by Chen et al. [8]. The gap depth, compressive strength of concrete, steel yield

strength, steel tube thickness, and load eccentricity were the main variables. Using ABAQUS software, a finite element model was created, and the output was compared to the outcomes of experimental tests. As the gap depth and load eccentricity rise, the strength of the CFHST columns was decreased. Additionally, due to the confinement effect, the thickness of the steel tubes increases the strength of the CFHST sections. Many researchers have examined the behavior of the CFHST columns [9–12]. These investigations have demonstrated that the axial load-strain relationships that exhibit compression behavior, axial stiffness, and post-peak behavior can be used to describe the behavior of CFHST columns under axial loading.

The performance of high strength CFHST rectangular columns was experimentally studied by Huang et al. [13]. CFHST columns with width-to-steel-plate thickness (B/t) ratios ranging from 18 to 68 were made by cutting steel plates into the required shapes and welding them together. Concrete had a compressive strength of up to 50 MPa while steel had a yield strength of up to 750 MPa. In rectangular steel boxes with high B/t ratios, local buckling was seen. Additionally, increasing the B/t ratio severely decreased the stiffness and capacity of CFHST columns. Experimental testing of CFHST columns with a centric static load was conducted by Tao et al. [14]. The main variables were the dimensions of the cross-section, the types of steel and concrete, and whether shear studs or internal rings were included. The results of the tests showed that the bond strength of stainless steel CFHST columns was lower than that of carbon steel. Welding an internal ring and shear connectors, the bond between the self-compacting concrete and the steel plates was increased. Yasser R. Tawfic et al. [15] investigated the characteristics of steel plate-reinforced concrete composite beams and concluded that the use of mechanical anchors increases the load bearing capacity of composite sections.

Using ABAQUS software to generate a finite element model, the compressive behavior of elliptical slender CFHST sections was examined by Dai et al. [16]. For accuracy and

validation, the software findings of the elliptical CFHST column were compared with those of the experimental tests. The researchers determined the buckling load of the elliptical sections of the CFHST columns in accordance with the requirements listed in Euro Code (EC-4). The elliptical CFHST section can be designed using the procedure outlined in the Eurocode to evaluate the axial compression behavior of the circular and rectangular CFHST sections.

This research aims to enable the designers to define the optimal design of the full-scale CFHST columns. Different variables were investigated such as the area of the longitudinal steel reinforcements and the area of the external steel tube, the shape of the cross-section, the T_s/b_s ratio, and the slenderness ratio.

2. Finite element idealization

Nonlinear finite element software ANSYS 18.1 was used to evaluate the overall behavior of the CFHST columns.

2.1. Element descriptions

Solid 65 simulates the concrete core elements that cracks under tension and crushes under compression. The element has eight nodes with three degrees of freedom at each node: translations in the nodal x , y , and z directions [17]. *Solid 185* is implemented to simulate the steel tube elements. *Solid 185* has eight nodes with three degrees of freedom at each node: translations in the nodal x , y , and z directions. The element has plasticity, hyper elasticity, stress stiffening, large deflection, creep, and large strain capabilities [17]. *Link 180* is adopted to simulate the steel reinforcement elements. The element is a uniaxial tension-compression element that has three degrees of freedom at each node: translations in the nodal x , y , and z directions [17].

3. Verification of the program

Nine CFHST columns, which were experimentally tested [18], were used to verify the finite element program (ANSYS 18.1). Table (1) and Figure (1) sketches the cross-section details for all investigated CFHST columns. All the tested CFHST columns have the same height (850 mm) and the same concrete compressive strength (25 MPa). Although all investigated columns have the same steel/concrete ratio (μ_s %), equal to 12.77%, they vary in steel area distribution, between internal reinforcement and external casing, in addition to cross-section shape and the depth to width ratio t_s/b_s . The geometry and specifics of the analyzed CFHST columns are presented in Figure (2). The elastic moduli of concrete and steel reinforcements (bars and tubes) were $E_c = 4400\sqrt{f_c}$ MPa and $E_s = 200$ GPa, respectively. The Poisson's ratio ν was 0.2, 0.3, and 0.3 for the concrete, steel bars, and steel tube, respectively.

3.1. Mesh idealization, loading, numerical parameters, and boundary conditions

To achieve desirable results, the mesh was considerably refined, and the model was constrained by the displacement condition, as shown in Figure (2). The applied boundary conditions simulated the experimental conditions of the module end. The applied load was divided among the top nodes of the

column. Finer increments were used in applying the static load. In this analysis, the convergence tolerance was set at (0.05) for displacement and force with a maximum iteration number of (15) to reduce the accumulation forces within the iteration. The contact between Solid185 (steel casing) and Solid65 (concrete core) was defined by the standard condition, which allows vertical sliding and separation between the two surfaces. The friction coefficient was set to 0.30 according to Lam et al. [19], and the contact cohesion was 0.01.

3.2. Analysis and comparison of the experimental with the theoretical results

Modes of Failure: Figure (3) shows the modes of failure for the theoretical and experimental CFHST columns. Generally, the failure modes obtained by the finite element analysis using ANSYS 18.1 were similar to those of the experimental results. The performed theoretical analysis and the experimental test results showed local buckling of the external steel tube within the lower or upper third as shown in Figure (3). Compatibly with the experimental modes of failure of the CFHST columns, the presence of longitudinal steel reinforcements and external steel tube exhibited a delay in the appearance of the local buckling compared with the columns without internal reinforcements.

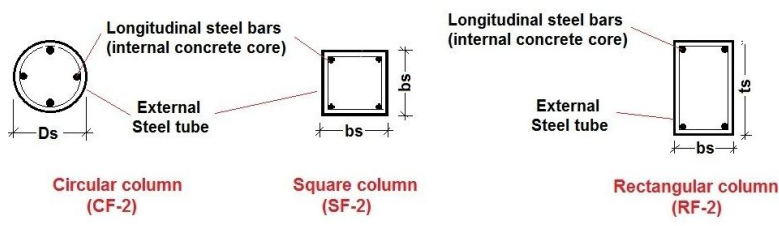


Figure (1): The geometry of the tested columns.

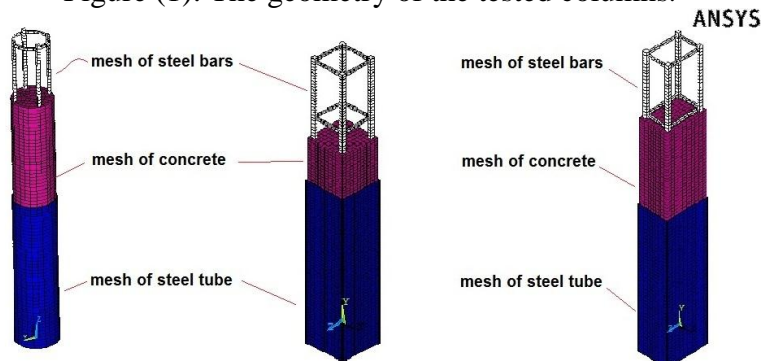


Figure (2): Meshing, location of load, and support of the model.

Table (1): Details and results of the experimental and the analytical results of CFHST columns [17].

Specimens	Dimensions(mm) $b_s \times t_s$	t_s / b_s	μ_{int} (%)	μ_{ext} (%)	Thickness of the Steel tube (mm)	Longitudinal Steel bars	Stirrups / m	Slenderness ratios	Ultimate loads experimentally (KN)	Axial displacement at ultimate load experimentally (mm)	$\frac{P_{ult} (theo)}{P_{ult} (exp.)}$	$\frac{\delta_u (theo.)}{\delta_u (exp.)}$
CF-1	Circle Dia.=135	---	0.00	12.7	4	-----	-----	25.2	906.0	12.69	1.02	0.96
CF-2			3.46	9.52	3	4 Ø 12	5Ø6		931.6	11.92	1.00	0.97
CF-3			4.73	7.84	2.5	8 Ø 10	5Ø6		947.3	9.60	1.01	1.14
SF-1	120 × 120	1	0.00	12.7	3.5	-----	-----	23.6	816.1	13.23	1.02	0.96
SF-2			3.56	8.88	2.5	4 Ø 12	5Ø6		876.2	12.84	1.04	1.01
SF-3			5.69	7.02	2	4 Ø 10 & 4 Ø 12	5Ø6		916.8	10.59	1.07	0.93
RF-1	100 × 144	1.4	0.00	12.7	3.5	-----	-----	28.3	513.2	11.02	0.98	0.94
RF-2			3.57	9.05	2.5	4 Ø 12	5Ø6		823.1	10.78	1.04	0.83
RF-3			5.70	7.14	2	4 Ø 10 & 4 Ø 12	5Ø6		874.5	7.54	1.01	0.94

μ_{int} : longitudinal steel bars ratio, μ_{ext} : steel tube ratio, $P_{ult (exp)}$: experimental ultimate loads, $P_{ult (theo)}$: theoretical ultimate loads, $\delta_u (exp)$: maximum displacement at ultimate loads (experimental), $\delta_u (theo)$: theoretical maximum displacement at ultimate loads.

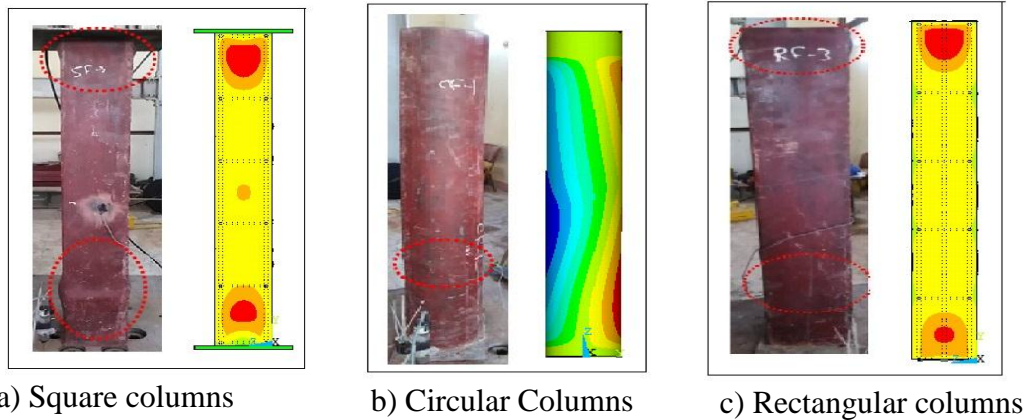


Figure (3): Experimental and ANSYS modes of failure for the CFHST columns.

Ultimate loads: The experimental and the theoretical results for all models are summarized in Table (1). Good agreement in the values of the ultimate load was detected for the finite element analysis and the experimental test results, with deviations ranges from -2% to $+7\%$. Columns having a constant steel reinforcement distributed between the internal concrete core and the external steel tube exhibited higher values of ultimate load capacity than those without internal longitudinal steel reinforcements.

Axial displacement curves: Figure (4) shows the experimental and the theoretical values of load–axial displacement. The finite element analysis highly agreed the behavior of the experimentally tested CFHST columns. The load-displacement curves showed two stages. The first stage from zero load up to the occurrence of the first local buckling. Slightly higher initial stiffness values were predicted that may be attributed to the effect of the considered boundary condition or modulus of elasticity of concrete. The second stage began at the first local buckling up to the column failure and it is characterized by a significant

reduction for the column stiffness. The analytical analysis shows ductile behavior similar to the experimental behavior of the

CFHST columns. Table (1) summarizes the the experimental and the theoretical axial displacement at the ultimate loads.

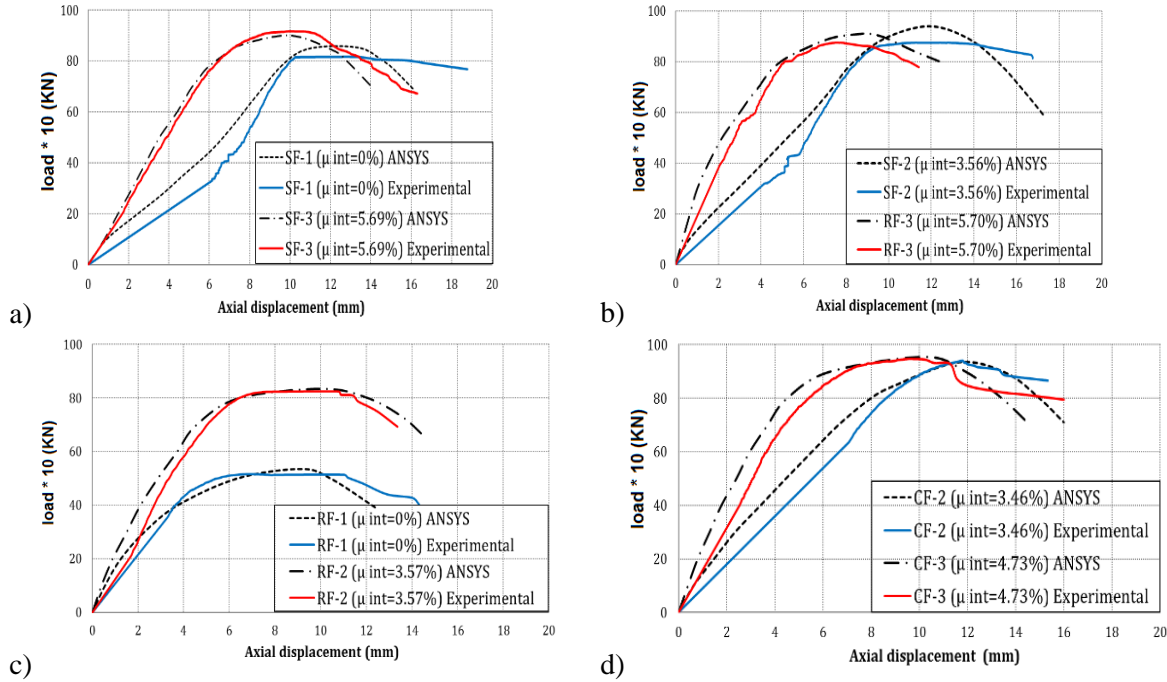


Figure (4): The experimental and ANSYS Load-displacement curves for the CFHST columns.

4. The Numerical Investigation Studies

4.1. Details of Theoretical Program

The properties of tested CFHST columns were numerically investigated using ANSYS (18.1) software. Table (2) shows the description of the modeled thirty-three CFHST specimens. The thirty-three columns were subsequently divided into two categories. The main variables of these categories were the distribution of the total steel area between the internal longitudinal steel reinforcement and the external steel tube, the cross-sectional shape (square, or rectangular), the depth to width (t_s/b_s) ratio, and the slenderness ratio (λ). The specimens label in Table (2) are designed based on the following rules: S, R1, and R2 represent the cross-section shape of the column that is square, rectangular with $t_s/b_s = 1.78$ and rectangular $t_s/b_s = 2.56$. The letter "D" refers to the steel distribution ratio, and the numbers after "D" are equal to 1, 2, and 3, representing an internal longitudinal steel ratio of 0%, 2%, and 4%, respectively. The numbers "3, 7.5, and 8.25" refer to the height of the CFHST columns (meter).

The first category comprised three conventional reinforced concrete (RC) columns and three CFHST columns filled with plain concrete. All columns in this category had the same height and cross-sectional area of the concrete and steel. The second category comprised twenty-seven columns that were subsequently divided into three groups. The nine columns in each group differed in their steel area distribution between core longitudinal reinforcement and external casing, and the slenderness ratio (λ).

4.2. The finite element idealization and material properties

The cross-sectional geometries, the mesh, the boundary conditions, the finite element models, and the loading of the analyzed CFHST columns are shown in Figure (5). For all columns, the yield strength of the steel tubes, steel bars, stirrups, and concrete compressive strength were 360 MPa, 360 MPa, 240 MPa, and 25 MPa, respectively. The materials properties and parameters were found to be suitable for the composite column analysis. the convergence tolerance was set at

(0.05) for displacement and force with a maximum iteration number of (15) to reduce the accumulation of forces within the iteration. The interface between Solid185 and Solid65 allows vertical sliding and separation between the the steel plate and the concrete core. The friction coefficient was set to 0.30, and the contact cohesion was 0.01.

4.3. Analytical Results and Discussion

4.3.1. Failure Modes

In the first category; the CFHST columns (CFHST-1, CFHST-2, and CFHST-3) were failed due to the occurrence of local buckling of the external tube and the crushing of the concrete core. However, the RC columns (RC-1, RC-2, and RC-3) failed due to the concrete crushing. The concrete was crushed near the top of the RC columns, whereas the CFHST columns buckled near the bottom (lower quarter) of the steel tube.

The failure modes of the analyzed CFHST columns of the second category are shown in Figure (6). Because of almost similar modes of failure for all the analyzed CFHST columns, so representative few output modes of failure are considered in this section. Generally, the failure modes were identical to the failure modes of the short columns in the first category (with a slenderness ratio ranging from 22.5 to 36); this may be due to the stress concentration. Overall buckling is the most common failure mode for all the long CFHST columns (with a slenderness ratio ranging from 56.5 to 99). The columns with internal longitudinal steel reinforcements showed a delay in the appearance of the local buckling or overall buckling compared to the columns without internal reinforcement. The presence of the local buckling for the majority of the square and rectangular short CFHST columns was in their lower-or-upper third sections.

Table (2): Details and results of the analyzed columns

Category	Specimens	Dimensions $b_s \times t_s$ (mm)	Steel tube thickness (mm)	Height (m)	Slenderness ratio (λ)	t_s/b_s	μ_{int} (%)	μ_{ext} (%)	$\mu_{S total}$ (%)	Longitudinal steel	Stirrups	Ultimate load (KN)	Axial Displacement at Ultimate load (mm)	
I	RC-1	450 x 450	----	3.50	25.9	1	4	---	4	16 Ø 25	5 Ø 8/m	3522	7.39	
	RC-2	319 x 635			36.6	2						3376	7.41	
	RC-3	259 x 782			45.0	3						3300	7.59	
	CFHST-1	450 x 450	4.4		25.9	1	--	4		----	----	4433	9.26	
	CFHST-2	319 x 635	4.1		36.6	2						4423	10.16	
	CFHST-3	259 x 782	3.8		45.0	3						4415	10.20	
II	S-D1-3	400 x 400	11.70	3.00	22.50	1.00	0.00	12.81	12.81		----	5 Ø 10 /m	7327.2	43.33
	S-D2 -3		10.00				2.00	10.80			8 Ø 22		8286.6	40.61
	S-D3 -3		9.00				4.00	8.81			10 Ø 28		8820.0	31.76
	S-D1 -7.5		11.70	7.50	56.25		0.00	12.81		----	7146.2		70.44	
	S-D2 -7.5		10.00				2.00	10.80		8 Ø 22	7681.8		64.45	
	S-D3 -7.5		9.00				4.00	8.81		10 Ø 28	8214.4		52.36	
	S-D1 -8.25		11.70	8.25	61.88		0.00	12.81		----	7007.1		68.25	
	S-D2 -8.25		10.00				2.00	10.80		8 Ø 22	7483.1		60.35	
	S-D3 -8.25		9.00				4.00	8.81		10 Ø 28	7895.2		52.43	

Category	Specimens	Dimensions $b_s \times t_s$ (mm)	Steel tube thickness (mm)	Height (m)	Slenderness ratio (λ)	t_s/b_s	μ_{int} (%)	μ_{ext} (%)	$\mu_{S\ total}$ (%)	Longitudinal steel	Stirrups	Ultimate load (KN)	Axial Displacement at Ultimate load (mm)	
R1	R1- D1-3	300 x 535	11.22	3.00	30.00	1.78	0.00	12.81		-----		6968.8	44.45	
	R1- D2-3		9.60				2.00	10.80		8 Ø 22		8104.7	41.53	
	R1- D3-3		7.93				4.00	8.81		10 Ø 28		8689.2	36.88	
	R1- D1-7.5		11.22	7.50	75.00		0.00	12.81		-----		6744.7	49.26	
	R1- D2-7.5		9.60				2.00	10.80		8 Ø 22		7500.0	48.76	
	R1- D3-7.5		7.93				4.00	8.81		10 Ø 28		8091.2	42.76	
	R1- D1-8.25		11.22	8.25	82.50		0.00	12.81		-----		6644.7	52.00	
	R1- D2-8.25		9.60				2.00	10.80		8 Ø 22		7300.0	51.67	
	R1- D3-8.25		7.93				4.00	8.81		10 Ø 28		7757.2	46.82	
	R2	R2- D1-3	250 x 640	10.45	3.00	36.00	2.56	0.00	12.81		-----		6431.4	46.06
		R2- D2-3		8.95				2.00	10.80		8 Ø 22		7800.8	42.48
		R2- D3-3		7.40				4.00	8.81		10 Ø 28		8518.4	38.54
		R2- D1-7.5		10.45	7.50	90.00		0.00	12.81		-----		6018.7	52.40
		R2- D2-7.5		8.95				2.00	10.80		8 Ø 22		7298.7	50.04
		R2- D3-7.5		7.40				4.00	8.81		10 Ø 28		7936.3	48.35
		R2- D1-8.25		10.45	8.25	99.00		0.00	12.81		-----		5793.7	46.89
		R2- D2-8.25		8.95				2.00	10.80		8 Ø 22		7128.7	52.52
		R2- D3-8.25		7.40				4.00	8.81		10 Ø 28		7593.7	45.64

b_s : width of columns, t_s : depth of columns, μ_{int} : internal steel ratio (longitudinal steel), μ_{ext} : external steel ratio (steel tube), $\mu_{S\ total}$: total steel ratio, λ : slenderness ratio

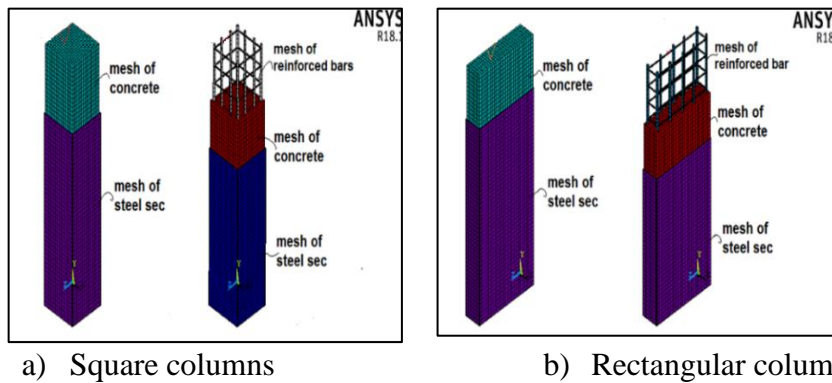
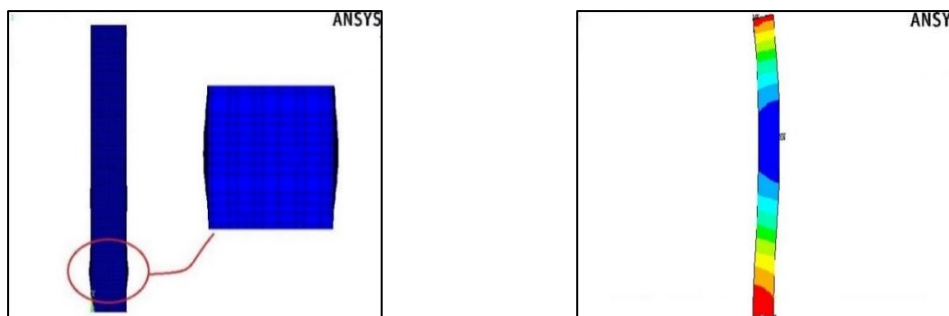


Figure (5): Cross-sectional geometries and meshing of FEA models of the CFHST columns.



a) Columns with slenderness (22.5 ~ 36) b) Columns with slenderness ratio (56.5 ~ 99)

Figure (6): Failure modes for analyzed CFHST columns.

4.3.2. Ultimate loads

Table (2) and Figure (7) show the values of the ultimate loads of the reinforced concrete and CFHST columns. The values of the ultimate loads for the CFHST columns in the first group were found to be up to 33% higher than the values of the ultimate loads of the reinforced concrete columns. The external steel tube increased the confinement and as a result the compressive strength of the concrete core.

The increase of the slenderness ratio of the square CFHST columns (from 22.5 to 61.88), the rectangular CFHST columns ($t_s/b_s=1.78$) (from 30 to 82.5) and the rectangular CFHST columns ($t_s/b_s=2.56$) (from 36 to 99) resulted in about 10% reduction for the values of the ultimate load. The value of the ultimate load for the rectangular CFHST column (R2- D1-3) (height 3 m – $t_s/b_s=2.56$) was about 12% lower than the values of the ultimate loads of the square CFHST columns (S-D1-3). For the CFHST columns that has a height equal 8.25 m, the value of the ultimate load of the rectangular cross-sectional column (R2- D1-8.25) (without internal reinforcement) was 17.3 % lower than that of the square column (S-D1 -8.25). However, the use of 4% internal reinforcements enhanced the efficacy of the

rectangular cross-sectional column (R2- D3-8.25) that showed 3.8% lower than the ultimate load of column (S-D3 -8.25).

For the studied slenderness-ratios of the square and rectangular cross-sections, the distribution of the total steel reinforcements between the concrete core and the external steel tube resulted in higher values of ultimate loads when compared with those of the CFHST columns have zero internal reinforcements. Increasing the percentage of internal reinforcements from 0% to be 4% resulted in 20.37%, 24.7% and 32.45% increase for the values of the ultimate load of the square column (S-D3 -3), rectangular column (R1- D3-3) and the rectangular column (R2- D3-3), respectively. The presence of 4% internal steel reinforcements for the CFHST columns (Height = 8.25m) resulted in 12.47%, 16.0% and 31.07% increase for the values of the ultimate load for the square column (S-D3 -8.25), rectangular column (R1- D3-8.25) and the rectangular column (R2- D3-8.25), respectively. The presence of internal steel reinforcements and the confinement effect of the external steel tube improve the concrete core's ability to withstand higher values of ultimate loads.

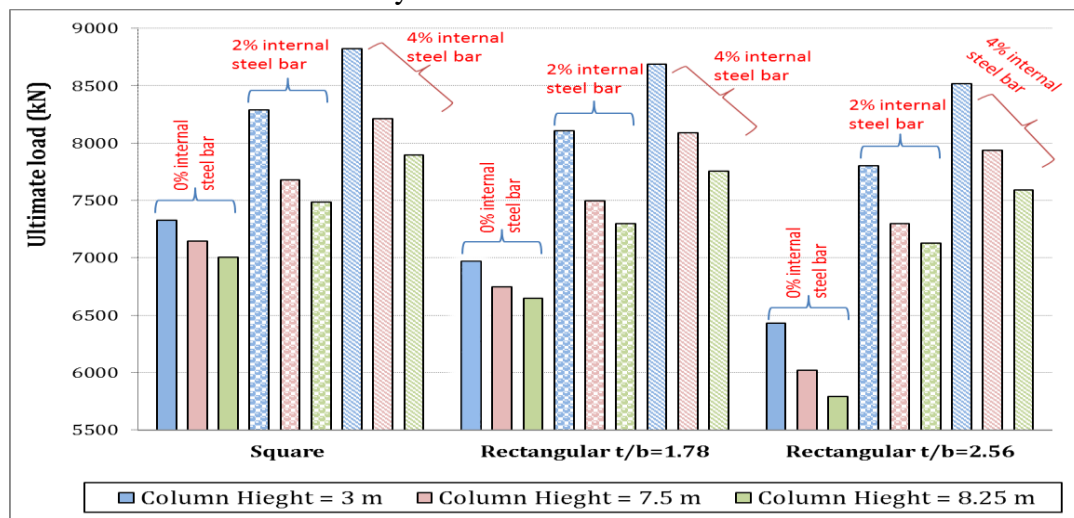


Figure (7): Ultimate load for CFHST columns under the effect of the distribution of the total steel and slenderness ratio.

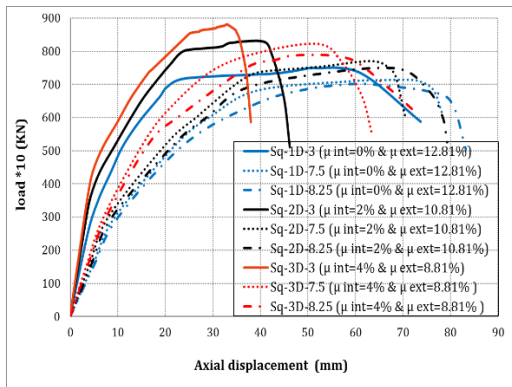
4.3.3. Axial displacement

The load–axial displacement relationships of the CFHST columns are plotted in Figure

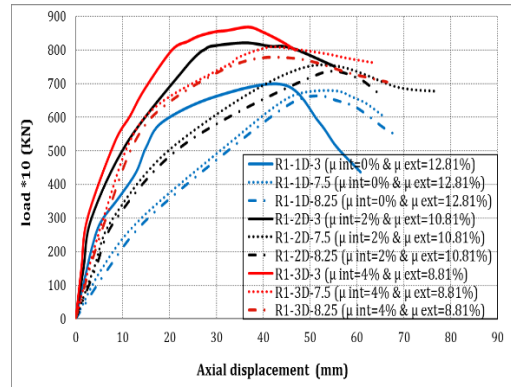
(8) showing the effect of the total steel area distributions and slenderness ration. The resulted axial displacement values at the ultimate load are presented in Table (2). The load-displacement curves for all columns exhibit three stages. Linear elastic deformations were occurred for the concrete and steel tubes in the first stage. In the second stage (plastic stage), some cracks in the concrete core begin to develop leading the steel tubes to buckle or overall buckling. The presence of internal steel reinforcement delays steel tube buckling, allowing the tube to maintain higher bearing capacity. In the third stage (failure stage), after reaching the peak load, the curves show sharp drops, indexing brittle failure.

As the internal steel reinforcement area increases, the stiffness of the core of the CFHST columns increases and as a result the axial displacements decreases. The application of 2% internal steel reinforcements resulted in a slight reduction in the longitudinal displacement values at the ultimate load. For CFHST columns that have a slenderness ratio ranging from 22.5 to 36, the presence of 4%

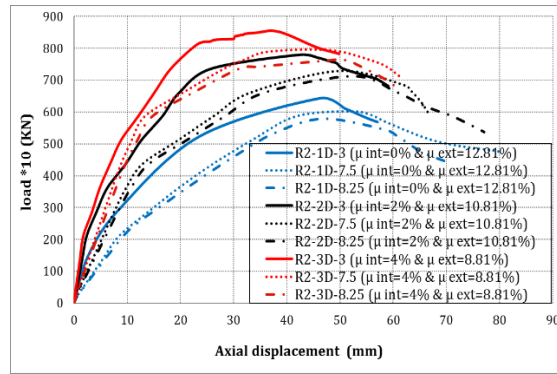
internal reinforcement results in 27%, 17%, and 16% reductions for the values of the axial displacements at the ultimate load of the square, rectangular ($t_s/b_s= 1.78$), and rectangular ($t_s/b_s= 2.56$) columns, respectively. The application of 4% internal steel reinforcements for columns with a slenderness ratio ranging from 56.25 to 99 results in 23%, 10%, and 3% reduction for the values of the vertical displacement at the ultimate load of the square, rectangular ($t_s/b_s= 1.78$), and rectangular ($t_s/b_s= 2.56$) columns. This reduction may be referred to the increased in the concrete core stiffness. In addition, increasing the slenderness ratio with increasing the depth to width ratio has very little effect on the values of the axial displacement at the ultimate load for the CFHST column. For all the loading stages, the increase of the slenderness ratio and the decrease of the stiffness resulted in an increase for the axial displacement for all the cross-sectional shapes of the columns.



a) Square CFHST columns



b) Rectangular CFHST columns ($T_s/b_s=1.78$)



c) Rectangular CFHST columns (Ts/bs=2.56)

Figure 8. Load–axial displacement curves for CFHST columns.

4.3.4. Ductility index

The ductility Index (*DI*) has been used to investigate the ductile behavior of CFHST columns [20]. The *DI* herein is defined as the following equation:

$$DI = \frac{\delta_{0.85}}{\delta_{y1}} \quad (1)$$

Where δ_{y1} is $1.33 \times \delta_{0.75}$ in which $\delta_{0.75}$ is the axial displacement at 75% the pre-peak load, and $\delta_{0.85}$ is the axial displacement when the post-peak load drops to 85% of the peak load. The *DI* of the analyzed CFHST columns was calculated and is presented in Figure (9). The distribution of the total steel area between the internal concrete core and the external steel tube increases the ductility index.

The use of 2% internal steel reinforcements for the square, rectangular (ts/bs= 1.78), and rectangular (ts/bs= 2.56) CFHST columns increases the axial compressive ductility index values by up to 5.28%, 50.15%, and 24.3%, respectively. However, the placement of 4% internal steel reinforcement for the square, rectangular (ts/bs= 1.78), and rectangular (ts/bs= 2.56) CFHST columns results in up to 9.1%, 61.7%, and 51.6% increase for the *DI*, respectively.

Increasing the slenderness ratio from 22.5 to 61.88 for the CFHST square columns have 0%, 2% and 4% internal reinforcements, the *DI* values were found to be reduced by 21.6 %, 23.5 %, and 21.7 %, respectively. Using 0 %, 2 %, and 4 % internal steel reinforcements for the rectangular (ts/bs = 1.78) CFHST columns,

increasing the slenderness ratios from 30 to 82.5 resulted in 42.7 %, 20 %, and 23.9 % reductions in the values of the *DI*, respectively. Increasing the values of the slenderness-ratio for the studied CFHST columns, the presence of internal steel reinforcements enhances the efficiency of the concrete core to resist higher values of axial loads and improves the ductility.

4.3.5. Strain in the steel tube

The load-tube strain relationships for the CFHST columns that have constant area of total steel reinforcements are shown in Figure (10). Generally, at a certain load and for all cross-sectional shapes and slenderness-ratios, the strain in the steel tube decreases with the increase of the internal steel reinforcement ratio. However, the ultimate values of steel tube strains were found to be increased with the increase of the internal steel reinforcements indicating high efficiency. The use of 4% internal steel reinforcement for the square columns (S-D3-3), (S-D3-7.5), and (S-D3-8.25) results in a 9.22%, 2.33%, and 4.58% increase for the values of the strain at the ultimate load, respectively. However, the placement of 4% internal steel reinforcements for the rectangular CFHST columns (R1-D3-3), (R1-D3-7.5), and (R1-D3-8.25), which have a width-to-breadth ratio of 1.78, results in considerable increase of 16.04%, 11.58%, and 4.38% in the strain at the peak load, respectively. Whereas, the rectangular CFHST columns (R2-D3-3), (R2-D3-7.5), and (R2-D3-8.25), which have a depth to width ratio of 2.56, resulting in a considerable increase of 36.80%, 16.71%, and 17.80% in the strain at the peak load, respectively.

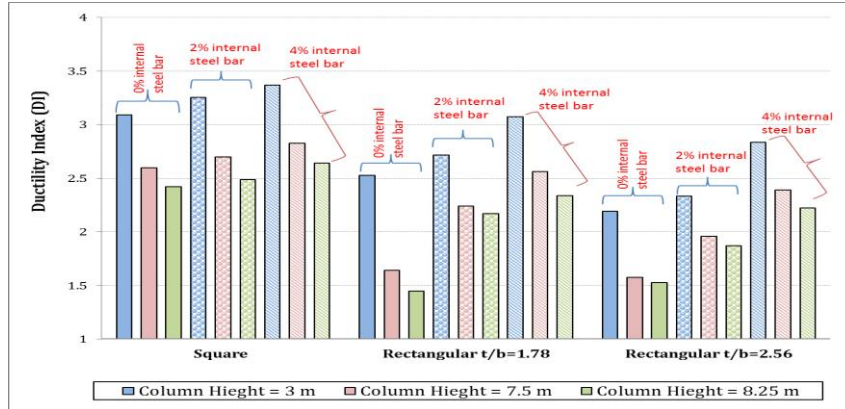
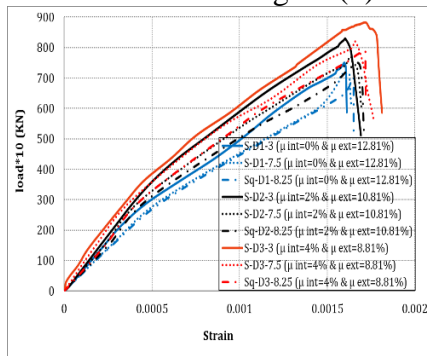
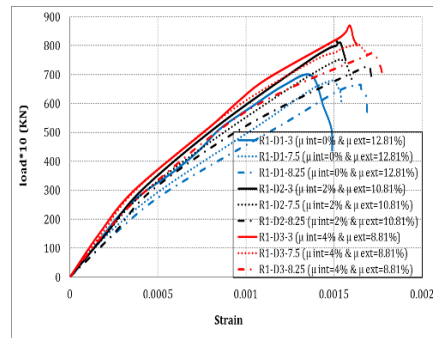


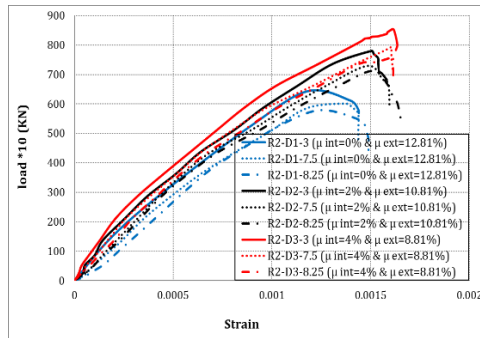
Figure (9): Ductility Index for CFHST columns.



a) Square CFHST columns



b) Rectangular CFHST columns (Ts/bs=1.78)



c) Rectangular CFHST columns (Ts/bs=2.56)

Figure (10): Load–strain curves of CFHST columns steel tubes.

Conclusions

1. The theoretical study showed that the failure mode for the CFHST columns, with a slenderness ratio ranging from 22.5 to 36, was due to local buckling in the steel tubes and crushing of the concrete cores; this may have been due to the stress concentration of the concrete core. Overall buckling is the most common failure mode for CFHST columns with a slenderness ratio ranging from 56.5 to 99. The columns with the total steel area distributed between the internal concrete

longitudinal reinforcement and the external steel casing show a delay in the appearance of local buckling or overall buckling.

2. Fixing the total steel reinforcements, The CFHST columns have internal steel reinforcements showed higher values of ultimate loads than the columns without internal reinforcements. The use of 4% internal steel reinforcement for the square columns (S-3D-3), (S-3D-7.5), and (S-3D-8.25) results in 20.4%, 14.9%, and 12.6% increase for the values of the ultimate loads,

respectively. However, the rectangular CFHST columns (R2-3D-3), (R2-3D-7.5), and (R2-3D-8.25), which have a depth to width ratio of 2.56, results in 32.5%, 31.9%, and 31.1% increase in the values of ultimate loads, respectively.

3. Having a slenderness ratio ranging from 22.5 to 36, increasing the internal steel reinforcement ratio from zero to 4% results in 27%, 17%, and 16% reduction for the values of the axial displacements at the ultimate loads of the square, rectangular ($t_s/b_s = 1.78$), and rectangular ($t_s/b_s = 2.56$) CFHST columns, respectively. Meanwhile, the use of 4% internal steel reinforcements for columns with a slenderness ratio ranging from 56.25 to 99 results in a 23%, 10%, and 3% reduction for the values of the vertical displacement at the ultimate loads of the square, rectangular ($t_s/b_s = 1.78$), and rectangular ($t_s/b_s = 2.56$) CFHST columns.

4. Having constant area of steel reinforcements, the placement of 4% internal steel reinforcement for the square, rectangular ($t_s/b_s = 1.78$) and rectangular ($t_s/b_s = 2.56$) CFHST columns results in up to 9.1%, 61.7%, and 51.6% increase of the ductility index, respectively. The presence of internal steel reinforcements and the confinement action of the external steel tube enhance the efficiency of the concrete core resulting in higher values of ductility index.

5. For a constant total steel area, increasing the internal steel reinforcement from zero to 4% results in 9.22%, 2.33% and 4.58% increase for the values of the strain in the steel tube at the ultimate loads for the square columns (S-D3-3), (S-D3-7.5) and (S-D3-8.25), respectively. However, the placement of 4% internal steel reinforcements for the rectangular CFHST columns (R1-D3-3), (R1-D3-7.5) and (R1-D3-8.25), results in a considerable increase of 16.04%, 11.58%, and 4.38% in the values of the steel tube strain at the peak load, respectively.

References

1. Kibriya, T. "Performance of concrete filled steel tubular columns." American Journal of Civil Engineering and Architecture 5, no. 2 (2017), pp.35-39.
2. AL-Eliwi, B. J.M., Ekmekyapar, T., AL-Samaraie, M. I.A., Hanifi, D. M. Behavior of reinforced lightweight aggregate concrete-filled circular steel tube columns under axial loading' Structures Journal, 16 (2018), 101-111.
3. Hassanein, M. F., M. Elchalakani, A. Karrech, V. I. Patel, and Bo Yang. "Behaviour of concrete-filled double-skin short columns under compression through finite element modelling: SHS outer and SHS inner tubes." Structures Journal, vol. 14, Elsevier, 2018 pp. 358-375.
4. Elchalakani, Mohamed, Mostafa Fahmi Hassanein, Ali Karrech, Sabrina Fawzia, Bo Yang, and V. I. Patel. "Experimental tests and design of rubberised concrete-filled double skin circular tubular short columns." Structures Journal, vol. 15, Elsevier, 2018, pp. 196-210.
5. Romero, Manuel L., C. Ibañez, Ana Espinós, José M. Portolés, and Antonio Hospitaler. "Influence of ultra-high strength concrete on circular concrete-filled dual steel columns." Structures Journal, vol. 9, Elsevier, 2017 pp. 13-20.
6. A. S. Abdel-zaher, L. M. Abdel-Hafez, Y. R. Tawfic and M. E. Abdel-fattah " Theoretical investigation of concrete field steel hollow section columns" Journal of Advanced Engineering Trends, Vol. 39, No. 1. January 2020, pp. 63-76.
7. Yang, Y. F., & Han, L. H. "Concrete filled steel tube (CFST) columns subjected to concentrically partial compression" Thin-Walled Structures, 50(1), (2012), pp.147-156.
8. Chen, S., & Zhang, H."Numerical analysis of the axially loaded concrete filled steel tube columns with debonding separation at the steel-concrete interface" Steel and Composite Structures, 13(3), (2012), pp. 277-293.
9. Zhao, X. L., & Packer, J. A. "Tests and design of concrete-filled elliptical hollow section stub columns" Thin-Walled Structures, 47(6-7), (2009), pp. 617-628.
10. Vidya, K. C., and George M. Varghese "Performance of Lean Duplex Stainless Steel Stub Columns with Stiffener." In

Applied Mechanics and Materials, vol. 857, pp. 171-176, (2016). Trans Tech Publications Ltd.

11. Ellobody, Ehab, Ben Young, and Dennis Lam. "Behaviour of normal and high strength concrete-filled compact steel tube circular stub columns." *Journal of Constructional Steel Research* 62, no. 7 (2006): pp. 706-715.

12. Giakoumelis, Georgios, and Dennis Lam. "Axial capacity of circular concrete-filled tube columns." *Journal of Constructional Steel Research* 60, no. 7 (2004): 1049-1068.

13. Huang, Z., Li, D., Uy, B., Thai, H. T., & Hou, C. (2019). Local and post-local buckling of fabricated high-strength steel and composite columns. *Journal of Constructional Steel Research*, 154, 235-249.

14. Tao, Z., Song, T. Y., Uy, B., & Han, L. H. (2016). Bond behavior in concrete-filled steel tubes. *Journal of Constructional Steel Research*, 120, 81-93.

15. Yasser R. Tawfic, Abdel-Nasser A. Soltan, Amr B. Saddek "Characteristics of steel plate-reinforced concrete composite beams subjected to flexural stresses" *Journal of Advanced Engineering Trends*, Vol. 41, No.2. July 2022: pp. 41-52.

16. Dai, X. H., Lam, D., Jamaluddin, N., & Ye, J. (2014). Numerical analysis of slender elliptical concrete filled columns under axial compression. *Thin-Walled Structures*, 77, 26-35.

17. ANSYS, Inc.: Element Reference for Release 18.1

18. Tawfic, Y. R., Sayed, A. S. A., Eid, M. A., & Abd El-Hafaz, L. M. (2021). Experimental Investigation to Evaluate the Behavior of Concrete-Filled Steel Tubular Columns under the Effect of the Distribution of the Total Steel Area between the Internal Concrete Core and the External Steel Tube. *International Journal of Engineering Research in Africa*, 54, 86-99.

19. Lam, D., Dai, X. H., Han, L. H., Ren, Q. X., & Li, W. (2012). Behaviour of inclined, tapered and STS square CFST stub columns subjected to axial load. *Thin-Walled Structures*, 54, 94-105.

20. Nabati, Amin, Tohid Ghanbari-Ghazijahani, and Ching-Tai Ng. "CFRP-reinforced concrete-filled steel tubes with timber core under axial loading." *Composite Structures* 217 (2019), pp. 37-49.